LA-UR-74-328

Conf-740613--1

VISCOUS MELT FLOW AND THERMAL ENERGY TRANSFER FOR A ROCK-MELTING PENETRATOR -- LITHOTHERMODYNAMICS

R. D. McFarland and R. J. Hanold*

ABSTRACT

The objective of the Subterrene program is to develop new, innovative systems for drilling and excavation based on the rock-melting concept. The development of rock-melting penetrators has advanced to the stage that it is necessary to be able to predict the relationships between applied thrust, power, surface temperature, and penetration rate for a wide variety of penetrator geometries and rock-soil mediums. These predictions are required to assess the practical limits of operation of various penetrators in different rocks and to aid in determining optimum penetrator shapes for specific excavation applications. The methods described herein represent a significant step to satisfy these analytical requirements. The basic operation of a melting penetrator in porous rock where the molten debris from the hole is disposed of by density consolidation is treated. Using a simplistic conduction analysis, optimum penetrator geometries are derived for the restricted case where local density consolidation prevails. The general problem is then formulated in terms of the two-dimensional Navier Stokes equations, energy equation, and the continuity equation with temperature dependent properties. These equations are cast in a general curvilinear, orthogonal coordinate system which corresponds to the typical melting penetrator shape. These equations are solved numerically and calculated results for required heated surface power, required thrust load, and the melt layer thickness distribution for a given penetration rate and surface temperature are presented for some typical penetrator geometries.

INTRODUCTION

The rock-melting excavation system that is being developed at the Los Alamos Scientific Laboratory is based on the concept of progressive local melting of rocks and soils to produce molten rock glass and a smooth lined hole. Rocks are mixtures of minerals and therefore, melting points are relatively low. The common igneous rocks, which are especially difficult to penetrate mechanically, in general become fluid at temperatures in the vicinity of 1470 K. Refractory metals, such as molybdenum and tungsten, have melting points much higher than this and are available for the development of the required rock-melting penetrator structures [1].

This proposed excavation method, which is relatively insensitive to variations in rock formation, produces a liquid melt whose behavior can be predicted by the laws of fluid mechanics. The basic rock heat transfer and melting processes are well defined

*Los Alamos Scientific Laboratory, Los Alamos, N.M.

and amenable to theoretical analyses and the rate of advance is dependent on the thermal flux supplied by the hot penetrator to the solid rock. The rock melt can be chilled to a glass and formed into a dense, strong, firmly attached hole lining as shown in Fig. 1. Thus by the use of a melting penetrator, permanently self-supporting holes can be produced even in unconsolidated sediments.

CONSOLIDATION PENETRATOR GEOMETRY ANALYSIS

The analysis and results to be presented in this paper are applicable to "melting-consolidation" Subterrene penetrators designed especially for making holes in porous rock or soft ground [2]. Because the glass-lining formed when the rock-melt cools is more dense and hence occupies a smaller volume than did the original porous rock, the molten debris from the hole can be entirely consolidated in the dense glass lining, thus completely eliminating the debris removal operation. The ratio of outer to inner radius of the melt layer is related to the properties of the rock by the conservation of mass which yields

$$\frac{r_m}{r} = \sqrt{\frac{1}{1 - \rho_R/\rho_L}} = \alpha \qquad (1)$$

or $r_m = \alpha r$ (density consolidation relation)

where r_m is the radius to the melting interface, r is the penetrator radius, and ρ_R and ρ_L are the densities of the in situ rock and rock melt respectively.

An analysis can be performed to optimize penetrator geometry under the assumption that the density consolidation relation is satisfied locally everywhere along the penetrator length. With reference to Fig. 2 the problem is characterized by an axisymmetric melting penetrator of arbitrary shape r(z) advancing into porous rock at a velocity V_z with the formation of a rock-melt layer whose outer radius is $r_m(z) = \alpha r(z)$. These surfaces are assumed to be isothermal with T_o being the surface temperature of the melting penetrator and T_m the melting temperature of the rock. The premise for the optimization is that each penetrator surface element dA conduct away the amount of energy required to heat, melt, and superheat the amount of in situ rock contained in an annular element of radius $r(z) + \epsilon$ and thickness dr_1 with the time scale for the problem being provided by the penetration velocity V_z.

The fundamental energy balance takes the form

$$Q_o = -\lambda_L \frac{dT}{d\eta} dA = 2\pi [r(z) + \epsilon] dr_1 V_z H$$

or (2)

$$Q_o = -\lambda_L \frac{dT}{d\eta} 2\pi[r(z) + \eta \cos\beta_o]ds = 2\pi[r(z) + \epsilon]dr_1 V_z H$$

where H represents the energy per unit volume which must be supplied to the rock. Heat conduction losses to the surrounding rock are neglected in this analysis. Rearranging the L.H.S. and integrating across the melt layer yields the following expression for Q_o if second order terms are omitted

$$\int_{\eta=o}^{\ell} \frac{Q_o \, d\eta}{r + \eta \cos\beta_o} = -\int_{T=T_o}^{T_m} 2\pi\lambda_L \, ds \, dT$$

or (3)

$$Q_o = \frac{2\pi\lambda_L \, (T_o - T_m) \cos\beta_o \, ds}{\ell n \left(\frac{\ell \cos\beta_o + r}{r} \right)}$$

where ℓ is the melt layer thickness in the normal (η) direction. The evaluation of the geometrical terms in the energy balance is presented in Appendix A with reference to Fig. 10. It should be noted that as r approaches zero, the melt layer thickness approaches zero and a disturbing singularity develops at the leading edge of the penetrator. This difficulty is avoided by increasing the melt layer thickness uniformly by a small amount, a, over its entire length. A residual melt layer thus exists at the leading edge and as the layer develops a becomes small compared to ℓ. A physical interpretation of this "standoff" distance results from the experimentally verified fact that unmelted quartz particles found in porous rocks, such as volcanic tuff, accumulate along the penetrator leading edge resulting in a small but finite melt layer thickness.

Utilizing the geometrical results developed in Appendix A, the energy balance becomes

$$\frac{Fp \, (\alpha + p^2)}{\alpha \, (1 + p^2)} = r \, A \, \ell n \, A \qquad (4)$$

where $p = \frac{dz}{dr}$

$$F = \frac{\lambda_L \, (T_o - T_m)}{V_z \, H} \text{ (physical parameter grouping)} \qquad (5)$$

$$A = \frac{\alpha(1 + p^2)}{\alpha + p^2} + \frac{1}{r} \left[\frac{ap \sqrt{\alpha^2 + p^2}}{\alpha + p^2} \right] \qquad (6)$$

Equation 4 is a first order, fourth degree ordinary differential equation which can be numerically integrated to yield the optimum penetrator geometry for a given set of parameters F, α, and a.

The solution domain of the differential equation is characterized by the following features. In general there exist two

solution curves for dz/dr, one for small values of r and one for large values of r. Each of these solution curves is double valued for dz/dr except at the vertical tangent point. The existence of a region between these curves where no solutions can be found indicates that the selected values of F and α are inconsistent with a physically realistic problem. This would be tantamount to specifying a penetration rate higher than can be obtained with the specified thermal boundary conditions or the inverse in which the penetration rate is too low and the melting interface would tend to move out beyond the radius specified by the density consolidation relation in Eq. 1. The solution procedure thus requires finding the value of F (for a specified value of a and α) which merges the solution curves across the range of r. This is illustrated in Fig. 3 which indicates the merging of these curves through the selection of F.

The penetrator geometry is now obtained by integrating the appropriate branches of the dz/dr solution curves. The combination of branches I and IV in Fig. 3 can be dismissed as an unphysical result while the combination of branches II and III produces a smooth "parabolic like" penetrator geometry. Calculated penetrator profiles for three different sets of conditions are illustrated in Fig. 4. The physical parameters corresponding to these conditions are listed in Table I.

TABLE I

VALUES OF PHYSICAL PARAMETERS

	a (mm)	α	ρ_R/ρ_L	F (mm)	λ_L (W/m•K)	$T_o - T_m$ (K)	H (j/mm^3)	V_z (mm/s)
"A"	2	1.3	0.408	2.60	2.5	500	2.04	0.24
"B"	2	1.5	0.556	3.00	2.5	500	2.78	0.15
"C"	2	1.7	0.654	3.41	2.5	500	3.27	0.11

As the in situ rock density increases (porosity decreases), a thicker melt layer must be formed for density consolidation of the molten debris and in addition more energy is required per unit volume of rock to accomplish the melting. For a given operating temperature difference and rock melt conductivity, these effects are directly reflected in the decreasing penetration rates that are calculated and the more slender penetrator geometries which have more heated surface area per unit frontal area of rock encountered. When the assumption of local density consolidation is relaxed, the general analytical problem of a heated penetrator advancing into solid rock requires a study of the nonlinear fluid mechanics of creeping viscous flow with high thermal flux energy interactions.

NON-LINEAR VISCOUS FLOW ANALYSIS

The calculational method presented here is based on the assumption that the effective "melt layer", i.e., the region in which the rock can be treated as a fluid "melt", is thin compared to the characteristic penetrator dimension. Calculations are made in two distinct regions: The melt layer is the primary calculation region in which the melt properties may vary with temperature.

The outer surface of the melt layer is termed the "melting interface" characterized by an arbitrary constant temperature and a lumped enthalpy change. For a medium with a distinct melting point, the melting interface temperature is the melting point temperature, and the lumped enthalpy change is the latent heat of fusion.

The second calculation region is the thermally affected "solid rock" outside the melting interface. In this region the medium through which the penetrator advances is considered to be a rigid body.

The melt in the region between the penetrator outer surface and the melting interface is treated as a homogeneous Newtonian fluid. Although extreme non-Newtonian behavior has been shown for at least one type of rock [3], this behavior is limited to a narrow range of temperatures near the melting point. Since there is little flow of the rock in this highly viscous regime, the assumption of a Newtonian fluid will be satisfactory for most applications. The effects of rock inhomogeneities, and the resulting melting temperature range observed in many geologic media, are included by employing temperature-dependent melt properties. In this way the latent heat of fusion can be expressed as an increased heat capacity over a temperature range rather than a lumped enthalpy change. The effects of thermal radiation can, in many cases, be simulated by employing an effective thermal conductivity which varies with temperature.

Geometries

Two general penetrator geometry types are considered in this computational method. The first is a simple, "solid" geometry in which the penetrator surface extends to the axis of symmetry at the leading edge (Fig. 5a). The second is the "annular" type geometry (Fig. 5b) for which no part of the penetrator reaches the axis of symmetry. This geometry type represents penetrators with a central coring or extrusion port. Only axisymmetric geometries are considered, but the particular profile of the surface is arbitrary within practical limitations.

Coordinate System

Figure 6 shows a representative portion of a heated penetrator surface and the associated melt layer. The frame of reference is fixed on the penetrator surface with solid rock approaching at a steady rate, i.e., at the penetration rate. The principal coordinate directions are: s, a meridional coordinate everywhere tangential to the penetrator surface in a plane through the axis of symmetry; and t, a nondimensional transverse coordinate across the melt layer which varies from zero at the penetrator surface to unity at the melting interface. With reference to previous notation: $t = \eta/\ell$. In general these constant-s lines are curved to be perpendicular to all constant-t lines from the penetrator surface to the melting interface.

Referring to Fig. 7, a unit differential volume of melt is given by $(\sigma ds)(\ell dt)(r d\theta)$, where ℓ is the total (dimensional) melt-layer thickness, r is the radial distance from the axis of

symmetry, θ the tangential dimension about the axis of symmetry and

$$\sigma = (ds^*/ds)_t = \sqrt{\left(\frac{\partial r}{\partial s}\right)_t^2 + \left(\frac{\partial z}{\partial s}\right)_t^2} \quad , \tag{7}$$

where s^* is the s-direction distance along any constant-t line, and z is a distance parallel to the axis of symmetry.

In most computations the melt layer thickness will change gradually with s, so that the angle difference, $\beta_m - \beta_o$, in Fig. 7 can be assumed to be small. With this assumption the constant-s lines are everywhere perpendicular to the penetrator surface across the melt layer, and:

$$\sigma = \sqrt{(1 + \ell t \omega_o)^2 + \left(t \frac{d\ell}{ds}\right)^2} \quad , \tag{8}$$

$$\tan(\beta_m - \beta_o) = \frac{d\ell}{ds} \Big/ (1 + \ell \omega_o) \quad , \tag{9}$$

where ω_o is the penetrator surface curvature:

$$\omega_o = - \frac{d\beta_o}{ds} \tag{10}$$

The melt-layer thickness, ℓ, is either specified or, for most practical applications, is calculated as a function of given thermal boundary conditions at each s-direction location. In general, the coefficients r and σ are functions of both s and t, while ℓ is a function of s only.

Physical Equations

The starting point for the differential equations used in the finite difference analysis are the general steady-state equations for the conservation of momentum, mass, and energy in orthogonal curvilinear coordinates [4]. These equations are cast in the present coordinate system and simplified by assuming: 1) $(\ell/R)^2$ is small compared to unity, where R is the characteristic penetrator dimension, and 2) The melt Reynolds Number $\bar{\rho} V_z \ell / \bar{\mu}$, is small compared to unity. Here, V_z is the penetration rate. Typical melt Reynolds Numbers are 10^{-8} to 10^{-4}.

Even though typical melt Prandtl Numbers range from 10^3 to 10^8, it can be shown [5] that for most applications body forces, work and viscous dissipation terms can be neglected. With the above assumptions, the differential equations are reduced to the following.

Equation of Motion, t-direction:

$$\frac{\partial p}{\partial t} = 0 \quad ; \quad \frac{\partial p}{\partial s} = \frac{dp}{ds} \tag{11}$$

Equation of Motion, s-direction:

$$\frac{\partial}{\partial t}\left[\sigma^3 r\mu \frac{\partial}{\partial t}\left(\frac{u}{\sigma}\right)\right] = \sigma r \ell^2 \frac{dp}{ds} - \sigma^2 r \ell^2 B \tag{12}$$

Energy Equation:

$$\frac{\partial}{\partial t}\left(\sigma r \lambda \frac{\partial T}{\partial t}\right) = \sigma \ell r c \rho v \frac{\partial T}{\partial t} + \ell^2 r c \rho u \frac{\partial T}{\partial s} - \sigma \ell^2 r Q''' \tag{13}$$

Continuity:

$$\frac{\partial}{\partial s}(\ell r \rho u) + \frac{\partial}{\partial t}(\sigma r \rho v) = 0 \tag{14}$$

The parameter Q''' in the energy equation is a lumped source term of energy rate per unit volume, which may include heat generation, viscous dissipation, work and thermal radiation. In Eq. 12 the body force per unit volume, B, in the s-direction is left in for generality.

In addition, an integral continuity equation is employed:

$$\psi = \left|\ell \int_o^1 r\rho u dt\right|_s = -\int_o^s [(\sigma r \rho v)_m - (\sigma r \rho v)_o] ds + \psi_{(s=0)} \tag{15}$$

where $2\pi\psi$ is the total s-direction mass flow of melt, and $s = 0$ at the leading edge. At the leading edge of a solid geometry penetrator r is zero. Along this singular line it can be shown that r can be replaced by σ in the differential equations. It can be seen that the differential equations are parabolic in that they are second order in the t-direction, but only first order in the s-direction, and that they are very similar to boundary layer equations.

Boundary Conditions

The applicable boundary conditions for the solution of the above equations for a free melting interface, are:

(a) $u(s,o) = 0$ (no slip at the penetrator surface)
(b) $u(s,1) = [\rho_R V_z/\rho(1)] \cos\beta_m$
(c) p specified at some s-direction point
(d) $v(s,o) = v_o$, $v_o = 0$ for no source or sink
(e) $v(s,1) = -[\rho_R V_z/\rho(1)] \sin\beta_m$
(f) $T(s,1) = T_m$, the melting interface temperature
(g) $-\lambda(1)\frac{\partial T}{\partial t}(s,1) = [V_z H_f \sin\beta_m + q_R]\ell$ (See below)
(h) $\frac{\partial T}{\partial s}(0,t) = 0$

If the melt layer thickness is not specified additional conditions are required:

(i) $T(s,o) = T_o(s)$ supplied
(j) $\frac{d\ell}{ds}(0) = 0$

If, in an annular geometry penetrator, the melting interface reaches the axis of symmetry some of the boundary conditions must be changed:

(b) is replaced by $\frac{\partial u}{\partial t}(s,1) = 0$

(f) & (g) are replaced by $\frac{\partial T}{\partial t}(s,1) = 0$

In this case the melt layer thickness is known and condition (i) must be supplied.

The heat flux from the melting interface into the thermally affected solid rock region [q_R in (g) above] is found by a separate solution of the energy equation in the solid rock region using the velocity components, $u = V_Z \cos\beta_m$ and $v = - V_Z \sin\beta_m$, of a rigid body. The solid rock region extends outward to a point where the outward heat flux is negligible, with the boundary condition that the temperature equals the in situ rock temperature at the outer edge of the solid rock region.

Method of Solution

The differential equations are solved by the technique of integration of known, or assumed, independent parameters over finite increments in t. The matrix of these numerical integrals, or sums, with the known boundary conditions is then solved for the unknown boundary conditions. To obtain the s-direction pressure gradient, the s-direction equation of motion is integrated three times to satisfy integral continuity. Details of the finite difference method are given in Ref. [5].

Since the equations are first order in the s-direction, explicit solutions may be obtained at each s-direction station consecutively. Iterations are required at each s-direction station due to the temperature dependence of the melt properties and because the melt layer thickness, ℓ, is an implicit parameter in all of the equations.

In performing the computations the penetrator surface geometry and surface temperature profile are prescribed, the melt properties are provided as functions of temperature and a penetration rate is imposed. Proceeding from the leading edge, numerical integrations are made in the t-direction at each s-direction station. These integrations yield the local t-direction distributions of u, v and T, the local melt layer thickness, s-direction pressure gradient, penetrator surface heat flux and shear stress, and the heat flux into the melting interface. Overall thermal energy, pressure and shear forces are then found by numerical integrations of local gradients in the s-direction.

COMPUTED RESULTS AND CONCLUSIONS

Calculations have been made with a computer program using these computational methods. These calculations covered a wide range of conditions for both simple and annular geometry penetrators in dense rock, for which material extrusion is required, and in porous rock for which density consolidation is possible with no material removal.

General conclusions agree with more approximate closed-form analyses. These conclusions include the essentially linear relation between required thermal power and penetration rate, and the high sensitivity of required thrust on penetration rate for a given penetrator surface temperature.

Figure 8 shows a map of operating conditions for a class of consolidating penetrators in local Los Alamos tuff of 48% porosity. The penetrators are of simple geometry with a parabolic-profile leading edge portion and a cylindrical heated aft portion whose length is that required to attain density consolidation at the aft end. In this geometry consolidation is attained only at the aft end of the heated section. In the forward portions of the penetrator the melt is extruded locally, i.e., the mean melt velocity relative to the penetrator is locally higher than the penetration rate. Fig. 8 is in the form of required thrust and total length required for consolidation as a function of penetration rate and penetrator surface temperature. The large advantage of high surface temperatures can be seen clearly. For a given surface temperature the required thrust is seen to vary approximately as the penetration rate to the 3.5 power.

Table II compares consolidating penetrators of the same overall heated length and diameter but of different profiles. The combination of a hemispherical leading portion and a cylindrical aft portion is seen to result in the highest penetration rate, but an extremely high required thrust. These characteristics are due to the rapid transition to the maximum penetrator diameter and a large amount of local melt extrusion in the forward end of the penetrator.

TABLE II

CALCULATED CONSOLIDATING PENETRATOR PERFORMANCE

Consolidating Penetrators

Length = 375 mm Diameter = 75 mm

Surface Temperature = 1800 K (Uniform)

Geometry	Penetration Rate (mm/s)	Thrust (kN)	Power (kW)
Hemisphere/Cylinder	0.59	490.	15.2
Parabaloid	0.22	1.5	6.7
Parabaloid/Cylinder (Parabola length = 184 mm)	0.40	14.0	12.0

The parabolic geometry, for which there is essentially no local melt extrusion, has a much lower penetration rate for the same heated length. The very low thrust is typical of this geometry and, in fact, the parabolic consolidator will always result in the lowest required thrust for a given penetration rate, but the longest required length. The combination of a parabolic forward section and a cylindrical aft section is seen to be a reasonable compromise geometry.

In Fig. 9 the location of the melting interface isotherm, in this case 1420 K, relative to an annular geometry penetrator is shown for three different imposed penetration rates. This represents a coring penetrator operating in porous rock and the melt does not reach the axis of symmetry for these conditions. At somewhat lower penetration rates, however, the entire core would be melted.

ACKNOWLEDGEMENTS

Sponsorship of this work by the National Science Foundation, Research Applied to National Needs, is gratefully acknowledged. This work was performed under the auspices of the U. S. Atomic Energy Commission.

NOMENCLATURE

A = surface area or term defined in Eq. 6
a = melt standoff distance
B = body force per unit volume
c = specific heat capacity
F = physical parameter grouping defined in Eq. 5
H = thermal energy per unit volume
H_f = latent heat per unit volume of solid rock
ℓ = melt layer thickness
p = geometry derivative in Eqs. 4-6 or melt pressure
Q = thermal conduction rate
Q''' = thermal power source per unit volume
q = heat flux, t-direction
R = characteristic penetrator dimension
r = radial dimension from axis of symmetry
s = curvilinear meridional coordinate along penetrator surface
T = temperature
t = transverse coordinate, nondimensional
u = s-direction velocity component relative to penetrator
v = t-direction velocity component relative to penetrator
V_z = penetration rate
z = axial dimension
α = consolidation radius ratio defined in Eq. 1
β = penetrator surface angle
ε = radial increment in conduction analysis
η = transverse coordinate perpendicular to penetrator surface
θ = coordinate about axis of symmetry
λ = thermal conductivity
μ = dynamic viscosity
ρ = density
σ = s-direction metric coefficient defined in Eq. 7
ψ = s-direction mass flow function
ω = penetrator surface curvature defined in Eq. 10

Subscripts

L = liquid rock (melt)
m = at melting interface
o = at penetrator surface
R = of in situ rock

REFERENCES

1. Hanold, R. J., "Rapid Excavation by Rock Melting - LASL Subterrene Program, "Los Alamos Scientific Laboratory Technical Report LA-5459-SR. Los Alamos, N.M: November 1973.

2. Neudecker, J. W., "Design Description of Melting-Consolidating Prototype Subterrene Penetrators," Los Alamos Scientific Laboratory Technical Report LA-5212-MS. Los Alamos, N.M: February 1973.

3. Shaw, H. R., Rheology of Basalt in the Melting Range, Journal of Petrology, 1969, 10(3), 510-35.

4. Hughes, W. F., and Gaylord, E. W., Basic Equations of Engineering Science, Schaum's Outline Series. McGraw-Hill, 1964.

5. McFarland, R. D., "Numerical Solution of Melt Flow and Thermal Energy Transfer for a Rock-Melting Penetrator," Los Alamos Scientific Laboratory Technical Report (to be published).

APPENDIX A

To develop the final differential equation (Eq. 4) used for penetrator geometry optimization, the geometrical interpretation of various terms in the energy balance must be developed. The basic constructions are illustrated in Fig. 10. At any location on the penetrator surface, an element of area dA has an outward normal in the η direction. The angle between the normal and the r direction is β_o and $\varphi = 90 - \beta_o$. The melt layer thickness in the r direction is $(\alpha - 1)r(z) + a'$ where $(\alpha - 1)r(z)$ is obtained from the density consolidation relation and a' is the radial projection of the residual melt layer thickness a. The normal melt layer thickness is ℓ where $\ell = \ell' + a''$, a'' being the normal projection of the residual melt layer thickness. As a result of the constant thickening of the melt layer, the melting interface is not parallel to the penetrator surface. In this analysis it is approximated by a straight line segment inclined at an angle τ from the radial direction or $\varphi-\tau$ from the penetrator surface element direction. The quantities to be determined are $\sin\beta_o$, $\cos\beta_o$, dr_1, ℓ and ϵ.

$$\sin\beta_o = \frac{1}{\sqrt{1 + p^2}} \quad , \quad \cos\beta_o = \frac{p}{\sqrt{1 + p^2}} \text{ where } p = \frac{dz}{dr} \qquad \text{(A-1)}$$

$$\cos(\varphi-\tau) = \frac{ds}{ds'} \quad , \quad \cos\tau = \frac{dr_1}{ds'} \quad , \quad dr_1 = \frac{\cos\tau\, ds}{\cos(\varphi-\tau)} \qquad \text{(A-2)}$$

With $\sin\beta_o = \cos\varphi$, $\cos\beta_o = \sin\varphi$, and $\Sigma dr = r(z)$ (penetrator radius)

$$\Sigma dr_2 = r_m(z) = \alpha r(z) = \alpha \Sigma dr \text{ and } dr_2 = \alpha dr$$

Since $\tan\tau = \frac{dz}{\alpha dr}$, $\tan\varphi = \frac{dz}{dr} = \alpha \tan\tau$ and Eq. A-2 becomes

$$dr_1 = \frac{\alpha \sin\beta_o \; ds}{\alpha \sin^2\beta_o + \cos^2\beta_o} \tag{A-3}$$

The normal and radial projections of the residual melt layer are determined as follows

$$\frac{(\alpha - 1)r}{\ell'} = \frac{(\alpha - 1)r + a'}{\ell' + a''} \quad \text{or} \quad a'' = \frac{\ell' \, a'}{(\alpha - 1)r} \tag{A-4}$$

$$a' = \frac{a}{\sin\tau} = \frac{a\sqrt{\alpha^2 dr^2 + dz^2}}{dz} = \frac{a\alpha}{p}\sqrt{1 + \left(\frac{p}{\alpha}\right)^2} \tag{A-5}$$

where $\ell' = \Delta - \delta$ and $\delta = \Gamma \tan(\varphi - \tau)$

$$\delta = \frac{(\alpha - 1)^2 \, r \, p}{(\alpha + p^2)\sqrt{1 + p^2}} \quad , \quad \Delta = \frac{r(\alpha - 1)\, p}{\sqrt{1 + p^2}} \tag{A-6}$$

and $$\ell' = \Delta - \delta = \frac{r(\alpha - 1)\, p\sqrt{1 + p^2}}{\alpha + p^2} \tag{A-7}$$

The normal melt layer thickness ℓ is given by $\ell = \ell' + a''$ where Eq. A-4 can be written as

$$a'' = \frac{a\alpha\sqrt{1 + \left(\frac{p}{\alpha}\right)^2}\sqrt{1 + p^2}}{\alpha + p^2} \tag{A-8}$$

and the projected radial distance ϵ is $\epsilon = \ell \cos\beta_o$ (A-9)

When these quantities are substituted in the energy balance, equations 4 through 6 are obtained.

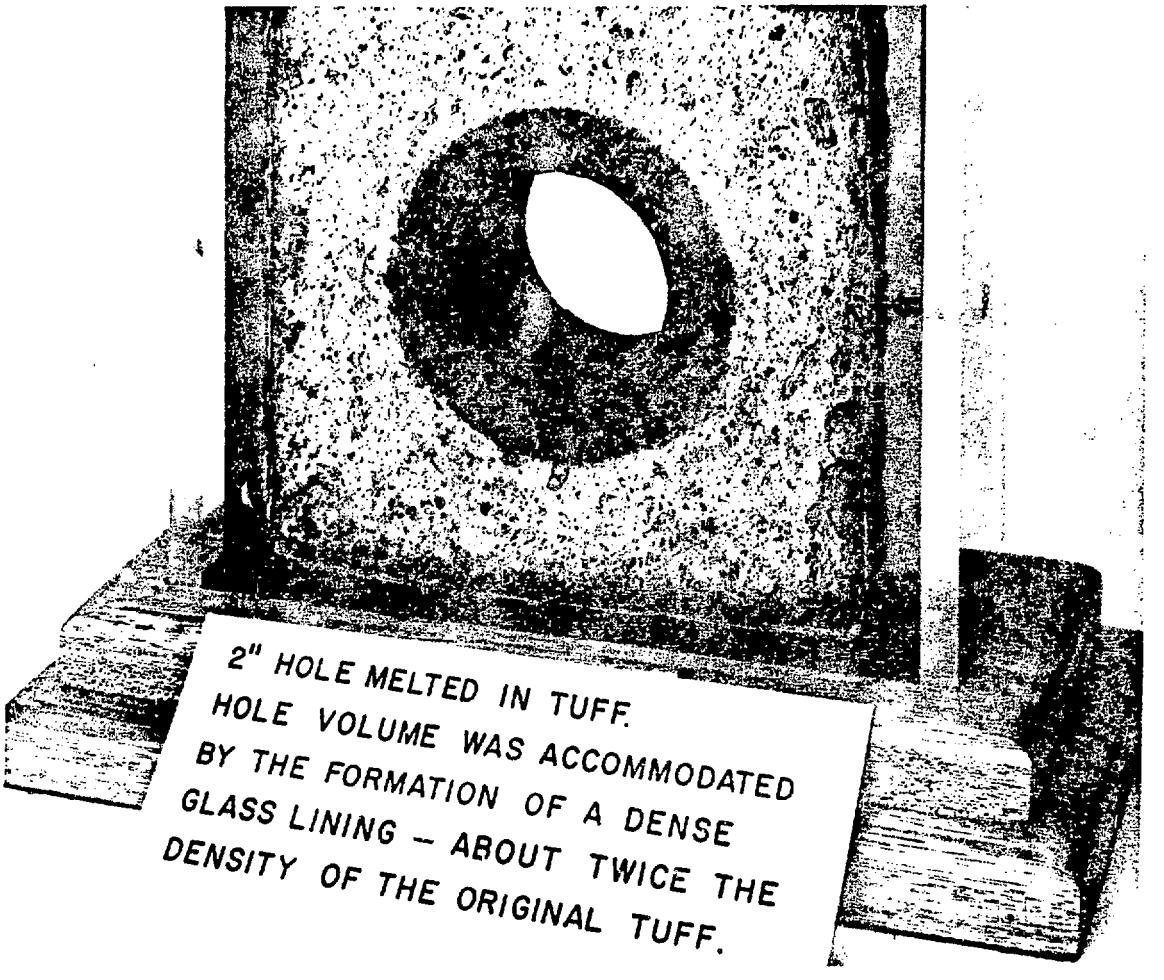

Fig. 1. Rock-glass lined hole in tuff produced by Subterrene melting penetrator.

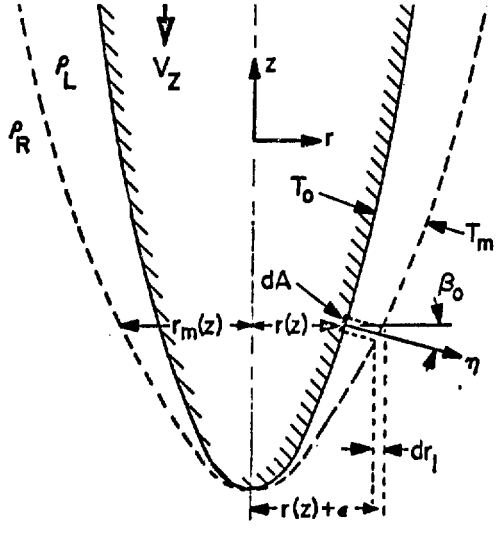

Fig. 2.

Density consolidation penetrator and melt layer configuration.

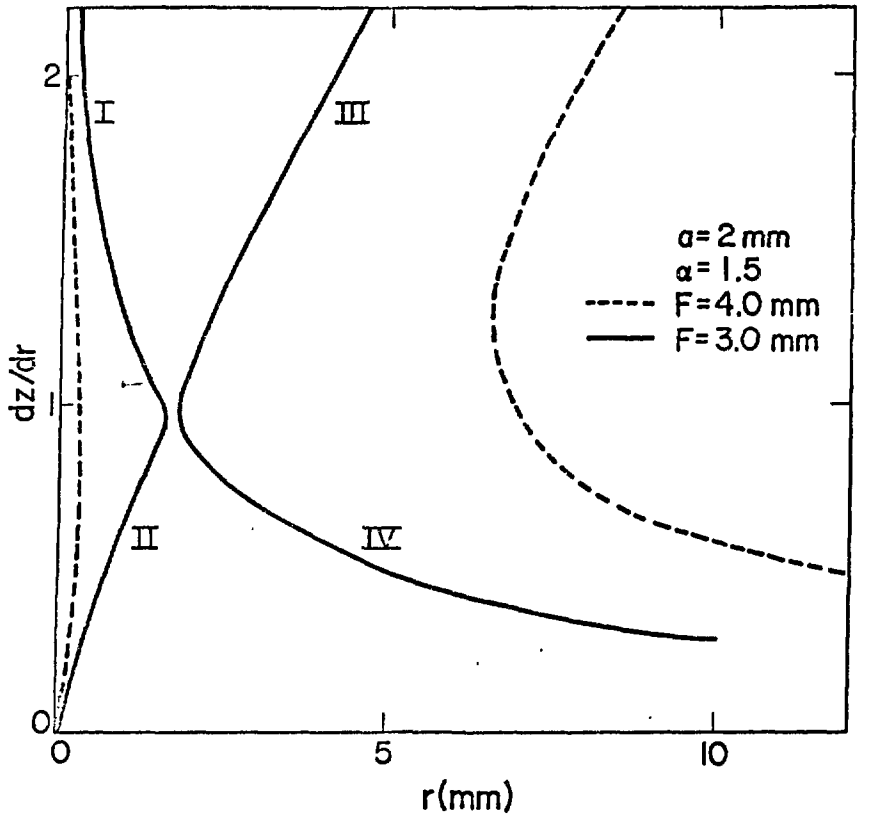

Fig. 3. Typical solution curves for Eq. 4.

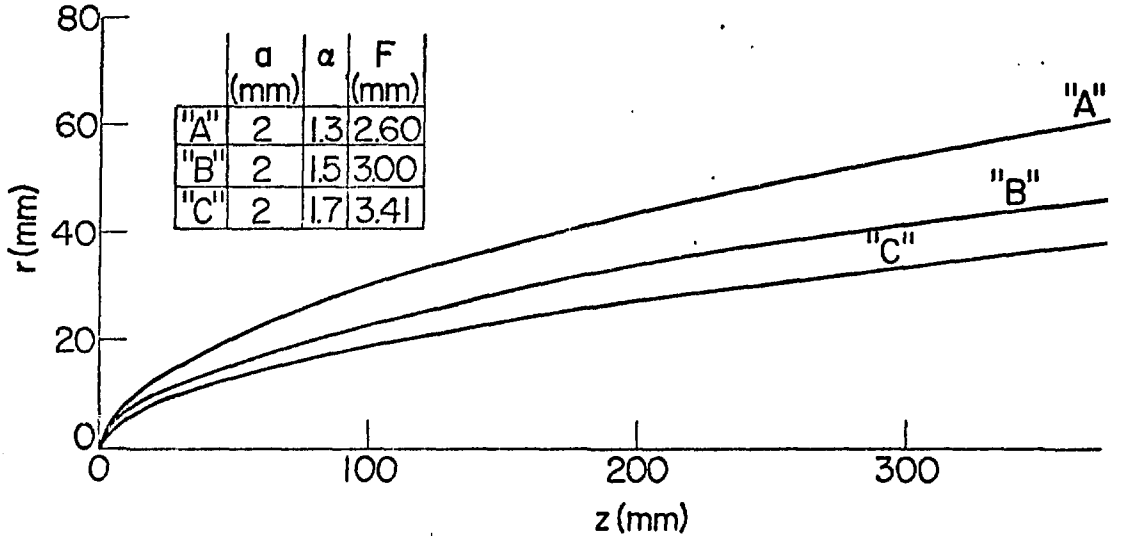

Fig. 4. Calculated density consolidation penetrator profiles.

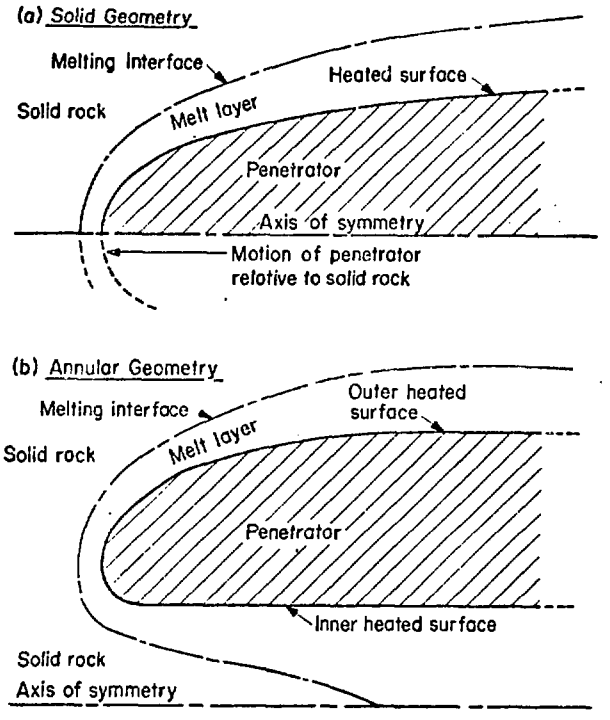

Fig. 5. Two classes of penetrator geometries - cross-sections in a plane through the axis of symmetry.

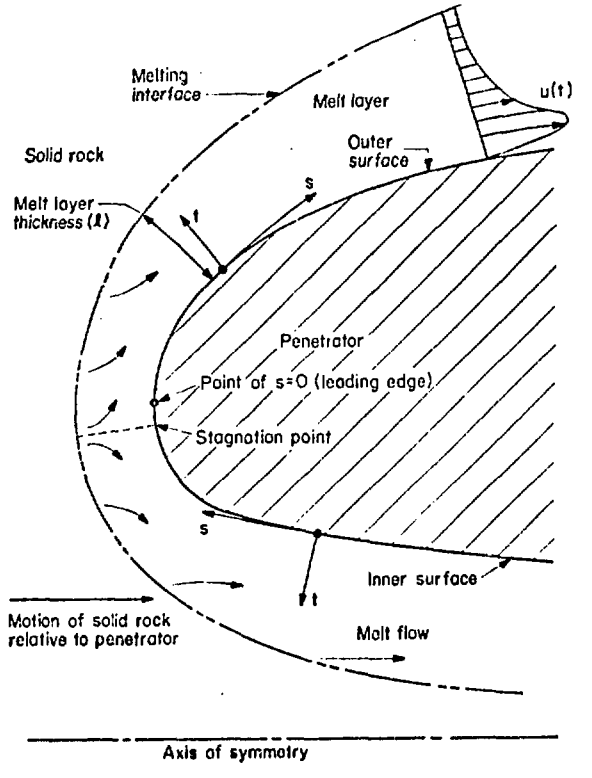

Fig. 6. Forward portion of an annular penetrator and associated melt layer showing the coordinate system fixed on the penetrator.

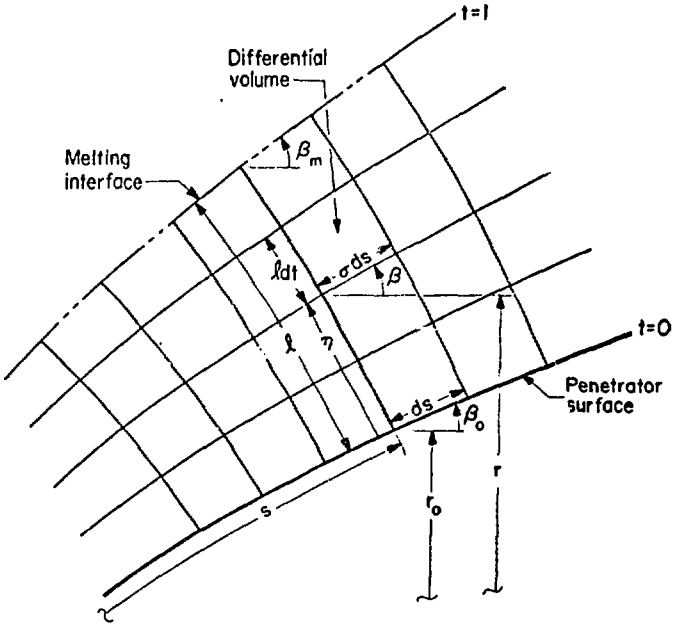

Fig. 7. An enlarged portion of the melt layer showing pertinent coordinate parameters.

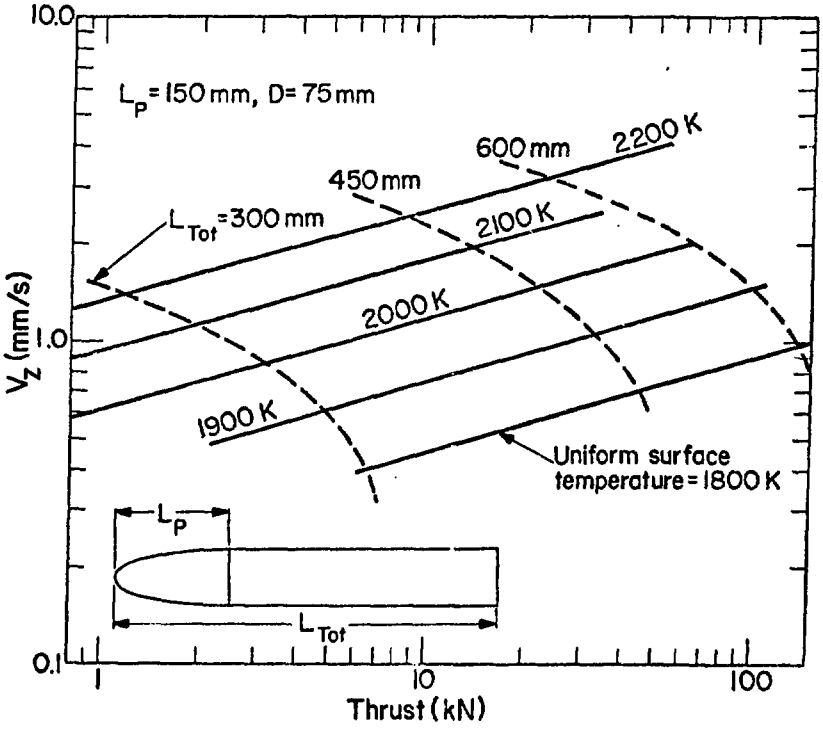

Fig. 8. Performance map for a class of solid consolidating penetrators operating in Los Alamos tuff.

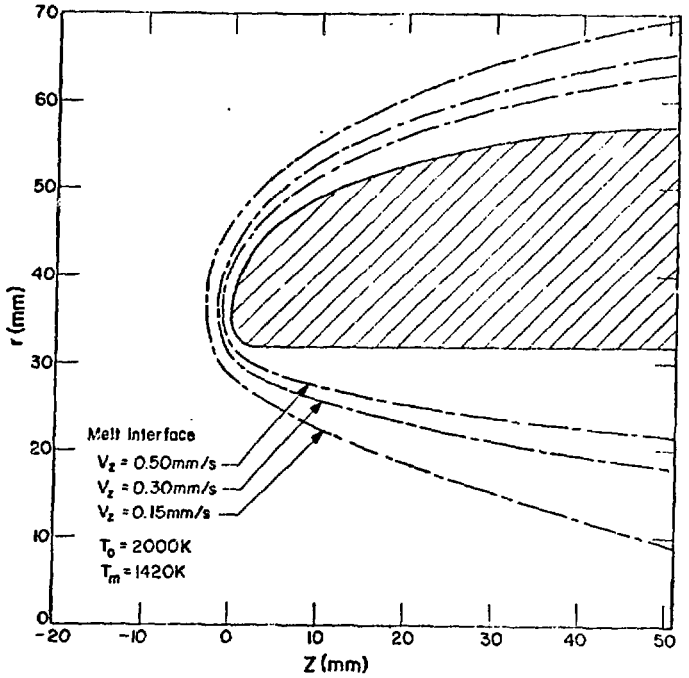

Fig. 9. Melting interface profiles at various penetration rates for an annular penetrator in porous rock.

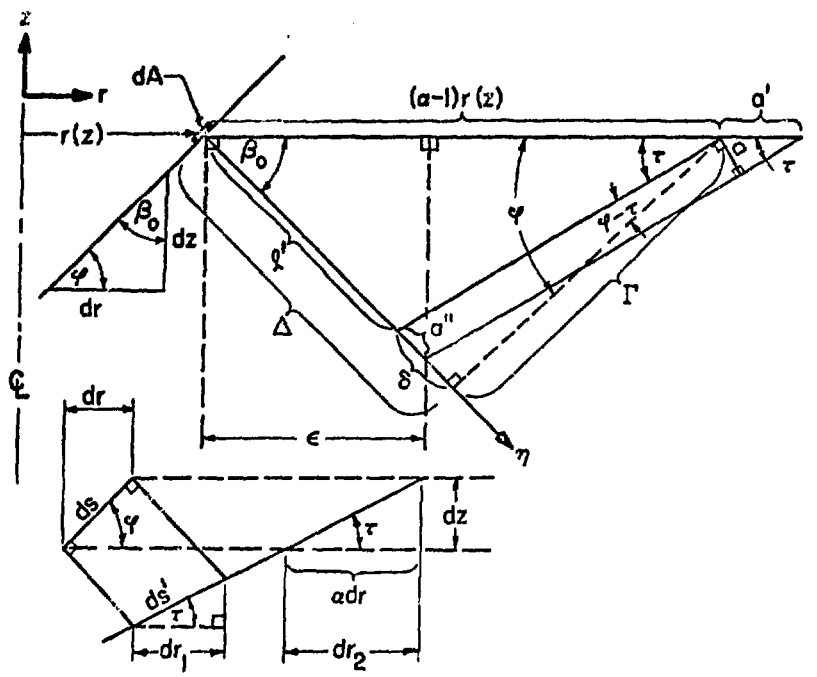

Fig. 10. Geometrical constructions used in penetrator geometry optimization calculations.